Journal Name

ARTICLE TYPE

Cite this: DOI: 00.0000/xxxxxxxxxx

Supplementary Information to: *HV-CVD Synthesis Yielding B-Doped SWCNTs with a Constrained Diameter Distribution*

Dido Denier van der Gon,*[a] Ramon Pinna–Brito,[a] Zhirui Liu,[b] Cauê S.C. Nogueira,[c] Yuhei Miyauchi,[b] Thomas Pichler,[a] Oliver H. Heckl,[a] and Paola Ayala*[a]

Received Date
Accepted Date

DOI: 00.0000/xxxxxxxxxx

This document contains supplementary information to the main manuscript. An overview of the B-doped carbon nanotubes, exclusively in single-Walled form, which have been reported in the literature is provided. Additional details related to the experimental conditions, as well as further spectral recorded on the materials only briefly described in the main manuscript can be found in this supplementary information document.

[a] *University of Vienna, Faculty of Physics, Boltzmanngasse 5, 1090, Vienna, Austria*
[b] *Institute of Advanced Energy, Kyoto University, Uji, Kyoto, 611-0011, Japan,*
[c] *The Polytechnic School, Arizona State University, Mesa, Arizona, 85212, United States*
E-mail: dido.denier.van.der.gon@univie.ac.at & paola.ayala@univie.ac.at

Supplementary Information

1 Availability of CBx-SWNTs

The main manuscript describes the peculiarities found using high-vacuum (HV) chemical vapor deposition (CVD) while synthesizing B-doped single-walled carbon nanotubes (CBx-SWNTs) with a given C and B-rich feedstock. In general, pristine single-walled carbon nanotubes (C-SWNTs) are highly attractive due to their optical, electronic and mechanical properties that originate from their one-dimensional structure. They have been synthesized in single-walled form for over decades with a number of methods. However, the same methods of synthesis can hardly be applied to make the CBx-SWNT counterparts. For instance, in CVD, the B reactivity with quartz tubes that are commonly used in CVD furnaces makes it a very complicated task that is otherwise almost standard for pure C tubes. The following table summarizes all the existing CBx-SWNTs reported in the literature to the best of our knowledge (compared to hundreds of publications on C-SWNTs). Regarding the doping levels, note that the highest B content reported corresponds to material made with substitution reactions, implying that a high percentage of B atoms are in BC_3 stable configurations, rather than in a substitutional configuration fashion. Also the formation of nanodomains [1] with this stoichiometry should be expected in those cases. On the other hand, 7% substitutional atoms have been reported as the highest doping level in CBx-SWNTs. This was done using a solid state precursor in HV-CVD [2], which is significantly different from all other works.

Method	**C/B Precursor**	**Doping level (%)**	**Reference**
Substitution reactions	SWCNT + B_2O_3	10-15	Borowiak-Palen et al. (2003) [3]
Laser ablation	Carbon paste + B	1.5-3	Gai et al. (2004) [4]
Laser ablation	Carbon paste + B	0.05-0.1	McGuire et al. (2005) [5]
Laser ablation	SWCNT + NiB	1.8	Blackburn et al. (2006) [6]
CVD	Triisopropyl borate	<1	Ayala et al. (2008) [7]
CVD	Triisopropyl borate	0.6	Daothong et al. (2009) [8]
Laser ablation	Carbon paste + B	0.3	Ayala et al. (2010) [9]
Substitution reactions/Laser ablation	SWCNT+B_2O_3	3	Panchakarla et al. (2010) [10]
CVD	Triisopropyl borate	<0.5	Ruiz-Soria et al. (2011) [11]
CVD	Triethyl borate	1.2	Monteiro et al. (2012) [12]
CVD	Triethyl borate	-	Ruiz-Soria et al. (2012) [13]
Substitution reactions	SWCNT + B_2O_3	-	Anand et al. (2013) [14]
Substitution reactions	SWCNT + B_2O_3	0.1	Fujisawa et al. (2018) [15]
Substitution reactions	B_2O_3	2.5	Panes-Ruiz et al. (2018) [16]
Substitution reactions	SWCNT + B_2O_3	1-3	Chiang et al. (2019) [17]
CVD	Sodium tetraphenyl borate	7	Reinoso et al. (2019) [2]
Substitution reactions	SWCNTs + B_2O_3	0.1-0.5	Liu et al. (2020) [18]

Table 1 Summary of the works reported in the literature, which focus exclusively on the fabrication of B doped nanotubes in *single-walled* configuration to the best of our knowledge. Noticeably, this is a very limited number compared to the vast literature on pristine C-SWNTs. [19]

2 Experimental design

The synthesis of CBx-SWNTs has been attempted in the past by many groups using standard CVD-methods but not significantly reported. This is likely due to limitations imposed by the chemistry involved in the processes in the presence of B. The largest problem is that the most commonly used furnaces in the experiments easily degrade due to the presence of B in the feedstock, presumably via formation of boron silicate within the often used quartz tubes, lowering the melting temperature of the reactors and eventually shattering. While designing our HV-CVD systems we tailored them in order to achieve different temperature gradients while controlling carefully the feedstock flow without any additional carrier gas. In the case of the experiments reported in our manuscript, we focused on working with the largest possible constant heat zone. As seen in the Figure 1, about 10cm could be kept constant from heating processes ranging between 200 to 950^{o}C as maximum temperature. The current intensities are only and indicative of the values at which we stabilized our system to work at given temperatures but this should, of course, vary from furnace to furnace and requires calibration.

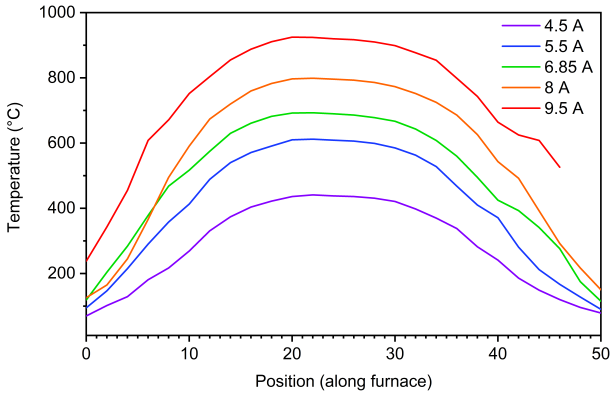

Fig. 1 The furnace temperature profile for different currents as a function of the position along the heating section.

3 Catalyst

Supported catalysts were used. The metal-containing compounds were mixed with the support material (MgO and SiO_2) and dissolved in ethanol (99.9% purity) via bath-sonication for 1 hour. The solution was stirred for 3 hours while kept at 50 °C. The mixture was subsequently kept at 40 °C overnight to dry and the resulting material was ground to a homogeneous powder and calcined for an additional hour. The compounds used for the catalysts are listed in the table below.

Catalyst	**Compounds**	**Support**
Fe	Iron acetate	MgO
Fe-Co[20]	Iron acetate & cobalt acetate	MgO & SiO_2
Fe-Mo	Iron(III) nitrate Ammonium heptamolybdate ∘ tetrahydrate	MgO
Co-Mo[21]	Ammonium heptamolybdate ∘ tetrahydrate Cobalt nitrate ∘ hexahydrate	MgO
Fe-Cu	Iron acetate & copper(II) acetate	MgO

4 Procedures and parameters

Note that in previous works, we reported the use of Iron Nitrate as an base of our catalysts highlighting the effective formation of CBx-SWNTs. The catalysts used in the present work are among the most efficiently used reported for pristine materials but the presence of new elements in the stoichiometry of the feedstock changes the scenario during the growth mechanism. This is why one key findings here highlights the method's robustness in producing material within a defined diameter range despite variations in catalyst composition and synthesis temperature. Notably, identical synthesis conditions applied to different catalysts yield highly similar material morphology, suggesting that the process is primarily feedstock-dependent. Optical absorption spectra shown in the main manuscript provide the overall diameter distribution observed in material obtained from different catalysts. The supporting data found in the graphs below correspond to Raman spectra recorded under different conditions. Note that Raman cannot provide an overall diameter distribution because it will reveal particularly the RBM signals that are in resonance with the specific excitation frequencies. However, it provides additional information that is valuable to understand the morphology of the samples.

The as-synthesised CBx-SWNTs samples were dispersed in a 2 wt% sodium deoxycholate (DOC) aqueous solution by tip sonication using a Branson SLP at 40% output power (60 W) for 2 hours. The dispersion was then centrifuged in a Thermo Scientific 120mx ultracentrifuge at 100'000 g for 30 minutes. The supernatant was collected and filtered three times using a Rotilabo syringe filter with a PTFE membrane and a pore size of 5 μm. These solutions were subsequently used for optical absorbance measurements.

4.1 Samples made with different catalysts at the same temperature

A combination of studies have brought us to conclude that working at 800C is a reliable temperature at which we safely grow single-walled material. While testing different catalysts at this temperature in presence of triisopropyl borate, the chiralities obtained lie close to each other. The final product that depends weakly on the catalyst, as thoroughly shown in the main manuscript.

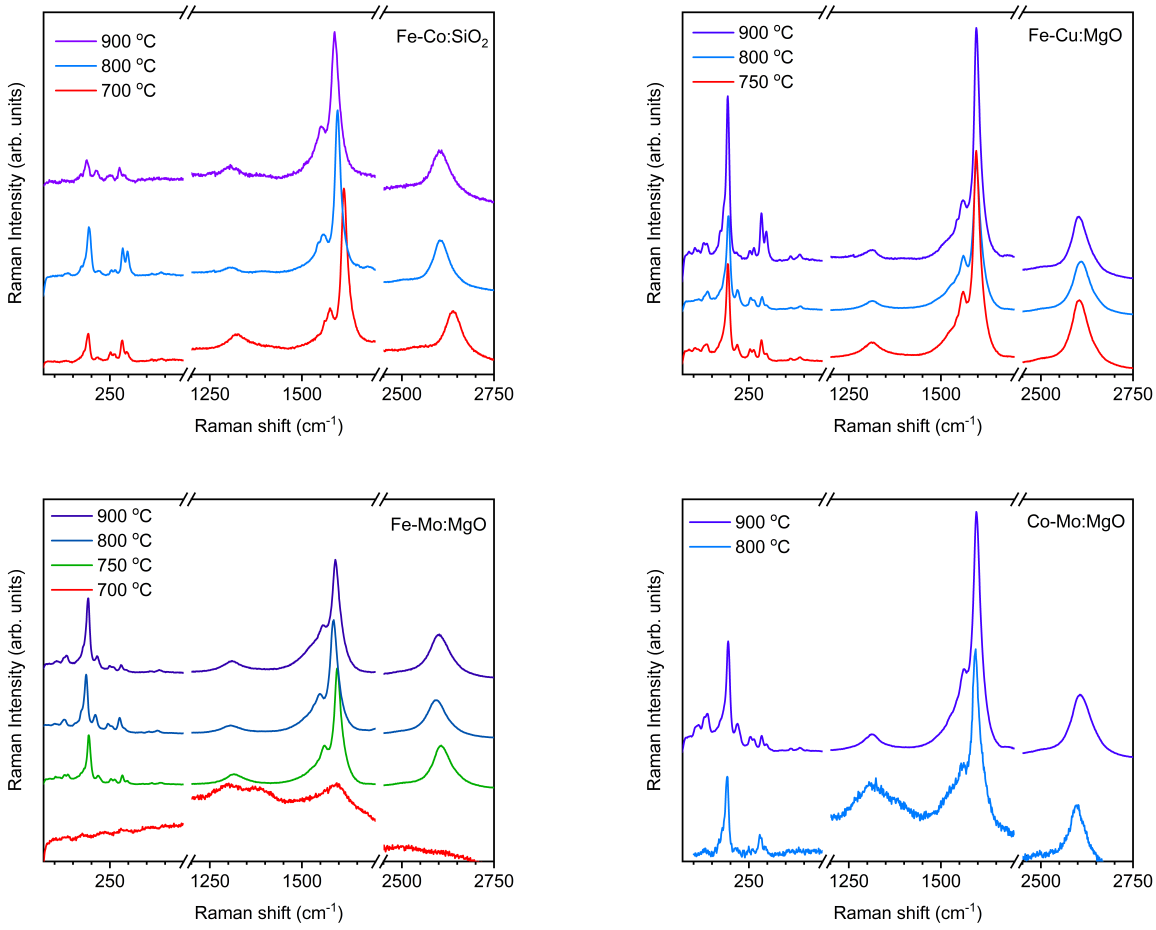

Fig. 2 Raman measurements performed on samples synthesized using specific catalysts over temperatures ranging from 700 - 900 °C

4.2 Influence of the temperature on the growth using the same catalyst

The temperature at which the growth occurs affects indeed the structure of the catalysts in general. The different melting temperatures in bimetallic catalysts usually limit the growth of pristine C-SWNTs. We have therefore paid careful attention to the growth trends using the 4 most efficient catalysts. The corresponding Raman spectra are shown below.

Fe-Co:MgO - The Raman results corresponding to this materials are shown extensively in the main manuscript. Figure 2 is a very complete information set recorded on these nanotubes. This catalyst consistently produced high-quality, high-yield samples over a wide temperature range. The corresponding Raman spectra show a very clear ID/IG ratio, which is a strong characteristic of the SWNT-material growth. The well defined Fano resonance features in the G line are almost invariant, indicating limited changes in the sample.

Fe-Co:SiO_2 - Most experiments using this bimetallic combination were carried out with catalysts supported on MgO, although a limited number of tests were also performed with catalysts supported on SiO_2. In the top left panel above, it is clearly observable that the synthesis was successful between 700 and 900 °C. For this and all other catalysts displayed, 700C is still low to grow high quality material, noticeable in the higher D band obtained from samples grown at higher temperatures. Following the same bi-metalic composition, and assuming minimal interaction with the supporting porous material, although the yield was significantly lower than for MgO-supported catalysts, the SiO_2-supported systems showed greater selectivity toward smaller diameters, with no tubes larger than 1.3 nm observed.[22]

Fe-Cu:MgO - It has been reported that Cu alone is not effective to grow C-SWNTs, but combined with Fe, it could enhance some specific chiralities.[23,24]. Among the four catalyst displayed in the figure 3, the corresponding Raman spectra exhibit the strongest signal for larger diameter tubes, compared to the other catalysts. At higher temperatures, the RBMs corresponding to smaller diameter nanotubes become more visible. Still, the diameter distribution is not altered as shown in the OAS of the main manuscript.

Fe-Mo:MgO - Samples synthesized with this catalysts, are only produced successfully from 750 °C onward. Additionally, the presence of thinner diameter tubes is the highest with this catalyst.[25] Additionally, the shape of the G line in the Raman response recorded from samples made at higher temperatures suggests the presence of more metallic tubes.[26]

Co-Mo:MgO - This was used to test the possibility to synthesize CBx-SWNTs using catalysts that do not contain Fe, although their yield and quality remain lower than those obtained with Fe-based systems. We further observe that samples grown with the Co–Mo catalyst are only successfully produced at higher synthesis temperatures. However there is a narrower diameter distribution at lower temperatures.[27]

4.3 Reproducibility of the experiments

In general, the method is robust with respect to variations of synthesis temperature and the diameter distribution remains within a defined range regardless the catalyst used. Furthermore, the reproducibility from batch to batch is high, yielding almost identical results for the material grown with each catalyst using different temperature. Most of our experiments were carried out using the Fe–Co:MgO catalyst, which consistently produced high-yield samples. Furthermore, Fe:MgO is a catalyst for which the sample quality is consistent. The Raman spectra corresponding to a series of experiments made under the same conditions are displayed in figure 3. The spectra have RBM proportions that are almost identical from batch to batch. The inset shows the ID to IG ratio, which is practically invariant. The change is minimal.

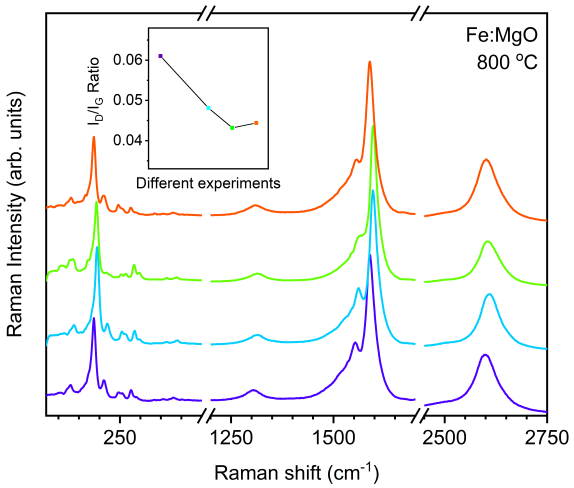

Fig. 3 Raman spectra for different experiments performed under the same conditions using Fe:MgO catalysts and a synthesis temperature of 800 °C.

Notes and references

1 D. L. Carroll, P. Redlich, X. Blase, J. C. Charlier, S. Curran, S. Roth, P. M. Ajayan and M. Rühle, Phys. Rev. Lett., 1998, **81**, 2332.
2 C. Reinoso, C. Berkmann, L. Shi, A. Debut, K. Yanagi, T. Pichler and P. Ayala, ACS Omega, 2019, **4**, 1941.
3 E. Borowiak-Palen, T. Pichler, G. G. Fuentes, A. Graff, R. J. Kalenczuk, M. Knupfer and J. Fink, Chem. Phys. Lett., 2003, **378**, 516–520.
4 P. L. Gai, O. Stephan, K. McGuire, A. M. Rao, M. S. Dresselhaus, G. Dresselhaus and C. Colliex, J. Mater. Chem., 2004, 669.
5 K. McGuire, N. Gothard, P. L. Gai, M. S. Dresselhaus, G. Sumanasekera and A. M. Rao, Carbon, 2005, **43**, 219.
6 J. L. Blackburn, Y. Yan, C. Engtrakul, P. A. Parilla, K. Jones, T. Gennett, A. C. Dillon and M. J. Heben, Chem. Mater., 2006, **18**, 2558.
7 P. Ayala, M. H. Rümmeli, T. Gemming, E. Kauppinen, H. Kuzmany and T. Pichler, Phys. Status Solidi B, 2008, **245**, 1935.
8 S. Daothong, J. Parjanne, E. I. Kauppinen, M. Valkeapää, T. Pichler, P. Singjai and P. Ayala, Phys. Status Solidi B, 2009, **246**, 2518.
9 P. Ayala, J. Reppert, M. Grobosch, M. Knupfer, T. Pichler and A. M. Rao, Appl. Phys. Lett., 2010, **96**, 183110.
10 L. S. Panchakarla, A. Govindaraj and C. N. Rao, Inorg. Chim. Acta, 2010, **363**, 4163.
11 G. Ruiz-Soria, P. Ayala, S. Puchegger, H. Kataura, K. Yanagi and T. Pichler, Phys. Status Solidi B, 2011, **248**, 2504–2507.
12 F. H. Monteiro, D. G. Larrude, M. E. Maia Da Costa, L. A. Terrazos, R. B. Capaz and F. L. Freire, J. Phys. Chem. C, 2012, **116**, 3281.
13 G. Ruiz-Soria, S. Daothong, T. Pichler and P. Ayala, Phys. Status Solidi B, 2012, **249**, 2469–2472.
14 B. Anand, R. Podila, P. Ayala, L. Oliveira, R. Philip, S. S. Sankara Sai, A. A. Zakhidov and A. M. Rao, Nanoscale, 2013, **5**, 7271.
15 K. Fujisawa, T. Hayashi, M. Endo, M. Terrones, J. H. Kim and Y. A. Kim, Nanoscale, 2018, **10**, 12723.

16 L. A. Panes-Ruiz, M. Shaygan, Y. Fu, Y. Liu, V. Khavrus, S. Oswald, T. Gemming, L. Baraban, V. Bezugly and G. Cuniberti, ACS Sensors, 2018, **3**, 79.
17 W. H. Chiang, Y. Iihara, W. T. Li, C. Y. Hsieh, S. C. Lo, C. Goto, A. Tani, T. Kawai and Y. Nonoguchi, ACS Appl. Mater. Interfaces, 2019, **11**, 7235.
18 Y. Liu, V. Khavrus, T. Lehmann, H. L. Yang, L. Stepien, M. Greifzu, S. Oswald, T. Gemming, V. Bezugly and G. Cuniberti, ACS Appl. Energy Mater., 2020, **3**, 2556.
19 M. H. Rümmeli, P. Ayala and T. Pichler, Carbon Nanotubes and Related Structures: Synthesis, Characterization, Functionalization, and Applications, Wiley-VCH Verlag GmbH & Co. KGaA, 2010, ch. 1, p. 1.
20 S. Maruyama, Y. Miyauchi, T. Edamura, Y. Igarashi, S. Chiashi and Y. Murakami, Chem. Phys. Lett., 2003, **375**, 553.
21 B. Kitiyanan, W. E. Alvarez, J. H. Harwell and D. E. Resasco, Chem. Phys. Lett., 2000, **317**, 497.
22 C. Fantini, A. Jorio, M. Souza, M. S. Strano, M. S. Dresselhaus and M. A. Pimenta, Phys. Rev. Lett., 2004, **93**, 147406.
23 M. He, B. Liu, A. I. Chernov, E. D. Obraztsova, I. Kauppi, H. Jiang, I. Anoshkin, F. Cavalca, T. W. Hansen, J. B. Wagner, A. G. Nasibulin, E. I. Kauppinen, J. Linnekoski, M. Niemelä and J. Lehtonen, Chem. Mater., 2012, **24**, 1796.
24 W. Q. Deng, X. Xu and W. A. Goddard, Nano Lett., 2004, **4**, 2331.
25 P. Dubey, S.-K. Choi, B. Kim and C.-J. Lee, Carbon lett., 2012, **13**, 99.
26 R. Saito and H. Kataura, Carbon Nanotubes: Synthesis, Structure, Properties, and Applications, Springer Berlin Heidelberg, Berlin, Heidelberg, 2001, p. 213.
27 S. M. Bachilo, L. Balzano, J. E. Herrera, F. Pompeo, D. E. Resasco and R. B. Weisman, J. Am. Chem. Soc., 2003, **125**, 11186.